Article

Assessing the Effectiveness of the Energy Storage Rule-Based Control in Reducing the Power Flow Uncertainties Caused by Distributed Photovoltaic Systems

Marco Pasetti

Department of Information Engineering, University of Brescia, Via Branze 38, 25123 Brescia, Italy; marco.pasetti@unibs.it; Tel.: +39-030-371-5939

Abstract: Battery energy storage systems (BESSs) are increasingly adopted to mitigate the negative effects caused by the intermittent generation of photovoltaic (PV) systems. The majority of commercial BESSs implement the self-consumption, rule-based approach, which aims at storing the excess of PV production, and then reusing it when the power demand of the loads exceeds the PV power generation. Even though this approach proved to be a valid solution to increase the self-consumption of distributed generators, its ability to reduce the power flow uncertainties caused by PV systems is still debatable. To fill this gap, this study aims at answering this question by proposing a dedicated set of key performance indicators (KPIs). These KPIs are used to evaluate the performance of a 13.8 kWp/25.2 kWh Lithium-Ion BESS coupled with a 64 kWp PV system. The results of the study revealed that the impact of the storage system had almost negligible effects on the uncertainty of the net power flows, while showing better results in terms of the reduction of the absolute power ramps, particularly during the BESS charge stages. These results represent an interesting point of discussion by suggesting that different storage control approaches should be investigated.

Keywords: photovoltaic; uncertainty; energy storage; net power flows; rule-based control

1. Introduction

The progressive paradigm shift towards distributed and decarbonized energy systems is heavily affecting the operation of modern power grids. In particular, the increasing penetration of the stochastic generation from renewable energy sources (RESs), particularly from photovoltaic (PV) systems, is calling for the adoption of new energy concepts, as well as smarter control architectures [1]. Distributed battery energy storage systems (BESSs), i.e., electrochemical energy storage systems installed directly at prosumers' premises, play a relevant role in this transition by supporting the integration of intermittent and stochastic RESs into distribution grids [2]. Despite the fact that they have been originally deployed to increase the self-consumption of RES generators installed in low voltage (LV) or medium voltage (MV) networks [3], the use of distributed BESSs has also been proposed to ensure the efficient and secure operation of distribution grids by providing multiple services, such as energy arbitrage, ancillary services, and active/reactive power control [4–6].

As will be discussed in detail in Section 1, despite several research studies in the literature proposing very different strategies and optimization algorithms for the charge and discharge control (or scheduling) of BESSs, the majority of commercial systems on the market implement the classic self-consumption, rule-based approach [7]. This control strategy aims at maximizing the self-consumption rate (SCR) of RES generators, i.e., the amount of energy produced by the RES generator and directly self-consumed by the user's loads, by storing the excess of RES production and then reusing it when the power demand of the loads exceeds the power generation of the RES.

Even though the self-consumption, rule-based approach proved to be a valid solution to reduce the amount of energy fed into the grid by distributed RESs, its ability to reduce

the power flow uncertainties caused by distributed RESs (in particular by PV systems) at the point of common coupling (PCC) with the main grid has never been studied. In addition, it must be noted that most of the studies in the literature assessing the impact of distributed PV generation on power grids focused their attention on voltage and/or frequency effects (such as voltage rise and voltage drops or frequency variations) [8–10], or on techno-economic evaluations [11–14], but none of them explicitly investigated the effect of distributed PV generation on the uncertainty of active power flows of prosumers. Indeed, this effect is usually not considered, while it represents a relevant input parameter for grid optimization systems, such as in optimal power flow (OPF) algorithms. Worth noting is the fact that most of the works in the literature make use of probabilistic approaches (such as the Monte Carlo algorithm) to take into account such uncertainties [15], since few real data are usually available.

To fill this gap, this study aims at assessing the effectiveness of the energy storage SCR increase aimed, rule-based control strategy in reducing the power flow uncertainties caused by distributed photovoltaic systems by proposing a dedicated set of key performance indicators (KPIs). These KPIs are then used to evaluate the effectiveness of a lithium-ion (Li-Ion) BESS in reducing the power flow uncertainties caused by a PV system. The study is based on the data collected for one month, with a time resolution of 5 min, from a 64 kWp PV system equipped with a 13.8 kWp/25.2 kWh Li-Ion BESS.

The structure of the study is organized as follows: in Section 2, the literature review on the assessment of the impact of PV and energy storage systems on distribution grids is presented by highlighting the novel contribution of the present study. Section 3 presents the reference use case and describes the system measurements. Section 4 defines the metrics and KPIs used to assess the impact of the PV and BESS on the uncertainty of active net power flows. Section 5 introduces the experimental dataset used in the study, while Section 6 presents and discusses the results of the analysis. Finally, in Section 7, the main findings of the study are summarized, and the conclusions are presented.

2. Literature Review and Contribution of the Study

As briefly discussed in the introduction, a large amount of works can be found in the scientific literature assessing the impact of distributed PV generation on distribution grids, and on advanced control approaches of distributed BESSs to mitigate such negative impacts. However, to the best of the author's knowledge, none of them focused on the assessment, particularly by means of real data, of the impact of distributed PV and storage systems on the uncertainty of the prosumers' power flows from a grid perspective. To better highlight this statement, in the following, the most recent and relevant studies on the topic are briefly presented and summarized.

Two relevant review articles addressing the management of stationary energy storage systems have been considered as main references to study the current topic. The first, authored in 2018 by Weitzel and Glock [16], proposed a systematic review of the literature on energy management for stationary energy storage applications. From this study, it is apparent that, despite a large amount of works being published during the last few years, investigating different strategies and algorithms for the optimal operation of BESSs (including residential PV-BESS installations), none of them investigated the ability of the traditional SCR increase aimed, rule-based control approach to reduce the uncertainties introduced by distributed PV systems. The second study, authored in 2019 by Baumann et al. [17], presented a review of very different multi-criteria approaches for evaluating the use of energy storage systems for grid applications by taking into account social, economic, technological, and environmental criteria of different types of energy storage technologies. However, the specific impact of the operation of BESSs on the volatility of prosumers' net power profiles was not considered.

More recently, following the increasing concern about the impact of the charging demand of electric vehicles (EVs) on the stability and operation of power grids, specific BESS management strategies have also been proposed to address the charging of EVs.

In [8], for instance, the simulated impact on the grid of the charging of EVs in the presence of distributed PV-BESS is presented by evaluating the rate of accelerated aging of grid components (e.g., transformers and voltage regulators). Even though the role of BESSs in mitigating the adverse impacts of EV charging on the grid is investigated, the impact of the rule-based strategy for the control of residential BESSs to reduce the uncertainty caused by PV systems is not considered.

The impact of PV installations on the voltage stability of distribution grids represents another relevant topic that has been largely studied in the literature. Among the broad research literature on the topic, the study proposed by [9] is worth mentioning, particularly concerning the use of metrics. In that study, a decentralized power management scheme was proposed to mitigate the impact of volatile PV and wind turbine (WT) generation on the grid voltage, and to improve the performance of grid-integrated BESSs. Similarly, [10] investigated the impact of distributed PV systems on the voltage quality in a low-voltage feeder in terms of the European standard EN 50160. The simulations are conducted with 10 min steps and comprise variable load profiles based on the Gaussian Mixture Model, and PV profiles based on experimentally obtained distribution parameters. An algorithm is proposed to determine the suboptimal energy storage deployment (the number of BESSs, placement, capacity, and rated output power) based on the voltage deviation minimization. Worth noting is the fact that, in both the referenced studies, the metrics adopted to evaluate the technical impacts of the simulated power management scheme are limited to the deviation of the voltage profile from the nominal value. In particular, the effectiveness of BESSs in reducing the uncertainty introduced by PV systems on a given load profile was not considered. Finally, focusing more generally on the disturbances introduced by distributed PV systems, [18] recently presented a BESS control approach to: (1) address abrupt disturbances caused by PV generators, and (2) shape the net load profile. The approach is based on BESSs coupled with PV generators equipped with proper controls. Simulations are carried out to demonstrate the effectiveness of the proposed BESS control by considering one daily load profile. Considerations about the daily variance of the considered metrics are not presented.

Concerning the use of storage systems for the maximization of the self-consumption of distributed RES generators, which is the main objective of the BESS control strategy considered by the present study, [7] proposed the comparison, carried out through simulations, of two different SCR increase aimed, rule-based strategies (i.e., the greedy and the feed-in damping strategy). However, the metrics considered in the study aim only at evaluating the efficient operation of the BESS (i.e., full equivalent cycles, efficiency, depth of cycles, resting periods, the number of changes of the sign, and energy throughput between changes of the sign), and do not consider the impact on the prosumer's power flows.

Other studies also considered the prioritization of loads by presenting both model predictive and rule-based control approaches aiming at taking into account (or maximize) the quality of service of customers, while minimizing the cost of the electricity bill. In [19], for instance, a model predictive control algorithm for PV-BESS installations is presented, aiming at minimizing the electricity bill (taking into account both the energy and the power peak component) by also implementing a series of device priorities to ensure the desired quality of service for the end user. Similarly, in [20], a rule-based load management scheme based on the classification of the criticality level of the loads was developed and tested for a residential PV-BESS installation by allowing the load prioritization and shifting based on certain rules. Worth noting is the fact that none of the referenced studies addressed the problem of the increased uncertainty of end users' power demand profiles caused by the installation of distributed PV generators.

Finally, specifically concerning the adoption of metrics for the assessment of the performance of BESS control strategies, [21] introduced a set of metrics composed by five indexes to evaluate the technical performances of load peak shaving, namely: Profile Flatness, Peak Duration, Exported Energy, Change Energy Demand, and Average Performance. Two peak shaving strategies are compared with the more usual self-consumption mode. However,

the effectiveness of the proposed strategies in reducing the volatility of the net power profiles is not considered.

Based on the presented literature review, it can therefore be noted that, to the best of the author's knowledge, a specific analysis based on real data of the impact of PV distributed generation and rule-based operating BESSs on the volatility of prosumers' active net power flows with the distribution grid was never discussed by the scientific literature. To fill this gap, the present study introduces the following contributions:

- Proposes a set of KPIs to evaluate the impact of distributed PV generators on the uncertainty of prosumers' net active power flows with the distribution grid;
- Proposes the use of such KPIs to assess the ability of BESS control strategies in reducing the power flow uncertainties caused by distributed PV systems;
- Presents an analysis of the ability of a BESS rule-based control approach in reducing the power flow uncertainties introduced by a PV system based on the data collected from a real PV system equipped with a Li-Ion BESS.

In particular, it must be noted that the proposed KPIs are defined independently from the BESS and PV power and/or system configuration, since they measure only the effects of the PV and BESS operation at the PCC with the main grid.

3. The Use Case

A public building located in the engineering campus of the University of Brescia, Italy, has been chosen as the reference use case. The building includes both department facilities (i.e., offices and classrooms) and student services, comprising dormitories, study halls, a cafeteria, a gym, and a baseball field. The building is connected to the local LV distribution grid and is equipped with a 64 kWp PV system, and a 13.8 kWp/25.2 kWh LiFePO$_4$ BESS. The BESS was installed as part of the research activities of the Energy Laboratory as University eXpo—eLUX of the University of Brescia, Italy [22]. Since the building in terms of power demand can be compared to a large residential building, and the PV systems are characterized by a relevant share of grid energy feed, the considered use case represents a significant scenario for the application of a stationary electrical storage system. Further information on the energy balance of the systems before the installation of the storage system was published in [23]. The system was designed with the aim of testing in the field the integration of BESSs into prosumers' systems equipped with new or existing PV installations. The BESS supervisory system was designed to allow the testing of simulated home energy management systems (HEMSs) and distribution management systems (DMSs) controls, while the monitoring system allows the evaluation of the performance of the system itself (e.g., by computing the charge, discharge, and round-trip efficiency) and the assessment of its impact on the prosumer's system and on the grid by making use of specific KPIs. To achieve this objective, according to the control architecture proposed in [24], the system allows the operation of three different control modes, namely: the classical rule-based algorithm (for the maximization of the PV self-consumption), the implementation of operational schedules provided by supervisory HEMSs, and the implementation of supervisory control requests provided by DMSs (e.g., for the provisioning of grid services, such as active and reactive power control capabilities). Last but not least, the system is also used to provide real-world data for the validation of BESS simulations, i.e., comprising both BESS lumped parameter models and simulated control functions. The design and implementation of the experimental control framework, as well as preliminary results on the BESS efficiency and on its impact on the prosumer's energy balance, was presented in [25]. Even though the project specification concerning the nominal capacity and the rated power of the BESS was limited by economical constraints, it must be noted that these have limited to negligible effects on the objectives of the experimental system, which are mainly focused on the test and analysis of BESS control functions.

3.1. The PV-BESS System Architecture

The PV-BESS system consists of a 64 kWp PV power plant formed by 18 PV strings connected to six three-phase PV string inverters. The PV plant is coupled with a 13.8 kWp/25.2 kWh LiFePO$_4$ BESS by means of an alternating current (AC)-coupled topology. It is worth noting that the LiFePO$_4$ technology represents one of the most diffused solutions for stationary BESS installations in Europe, while the AC-coupled topology is largely adopted in PV-BESS applications, because it can be easily retrofitted to existing PV systems and features a high flexibility in terms of system configuration [26]. A detailed description of the PV-BESS architecture is provided by the schematic diagram of Figure 1.
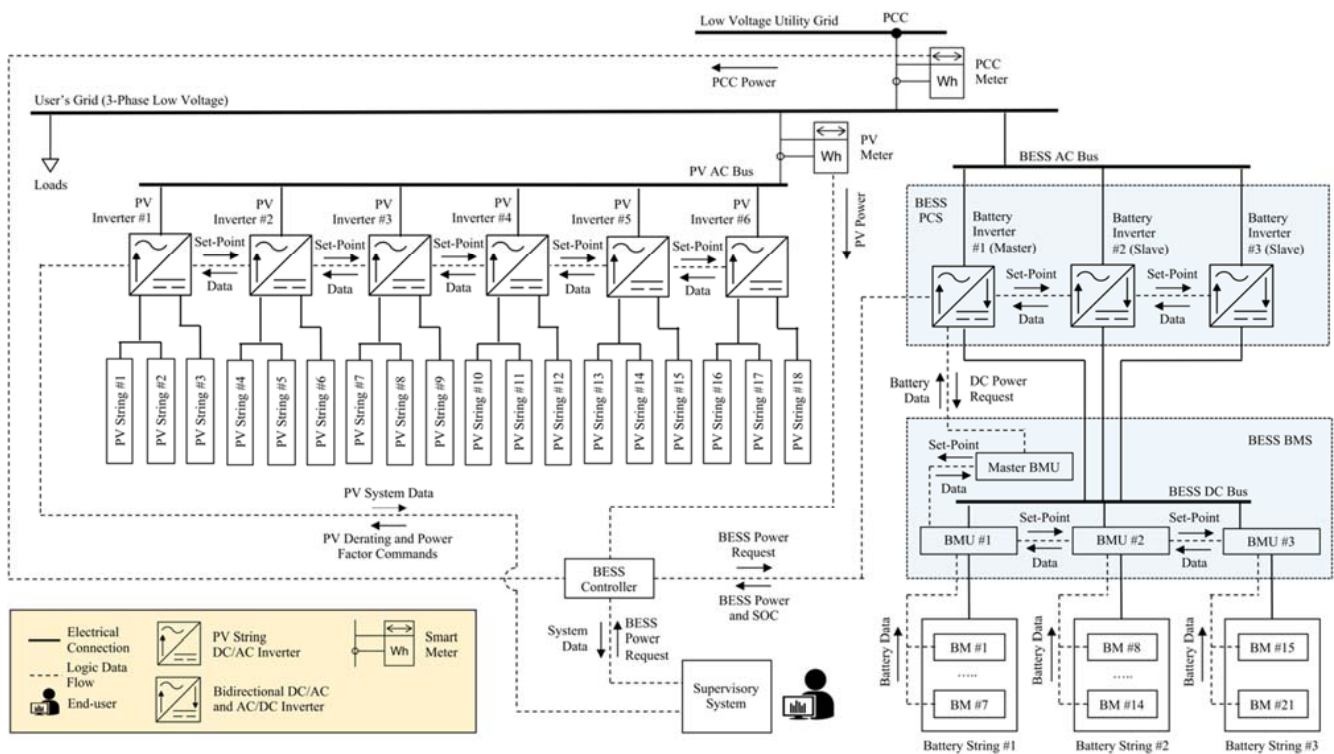
Figure 1. Schematic layout of the PV-BESS system architecture. PV: Photovoltaic, BESS: battery energy storage system, BMS: battery management system, BM: battery module, BMU: battery management unit, PCS: power conversion system, PCC: point of common coupling, AC: alternating current, DC: direct current, SOC: state of charge.

The BESS is formed by three battery strings (BSs), each containing seven battery modules (BMs), each with a 1.2 kWh rated capacity, connected in parallel. The battery management system (BMS) is formed by three battery management units (BMUs) and one master BMU. The BESS power conversion system (PCS), i.e., the system responsible for the AC to direct current (DC) and DC to AC conversion, is formed by three single-phase bidirectional inverters, with one inverter configured as the master device. Both the PV and the BESS inverters are connected to the LV PCC with the main grid.

The system is equipped with a BESS controller, which provides charge and discharge control requests to the BESS PCS, depending on the active power generation of the PV system and on the active power measurement at the PCC. The BESS controller communicates with the BESS master inverter via Modbus TCP/IP. The power flow measurement at the PCC and PV are provided by two power meters (i.e., the PCC meter and the PV meter, respectively) communicating with the BESS controller via Modbus TCP/IP. The entire system was implemented by making use of commercially available equipment. All of the devices are connected to an Ethernet switch linked to the local area network (LAN).

The BESS controller implements the typical rule-based control approach by charging the batteries with the excess of power generation of the PV system (limited to the charge

rated power of the BESS) until the BESS reaches the maximum allowed state of charge (SOC), usually set to 100%, and by discharging the batteries with the excess of power demand of loads (limited to the discharge rated power of the BESS) until the BESS reaches the minimum allowed SOC, usually set between 10 and 20%. In the considered use case, the maximum and minimum SOC values were set to 100% and 20%, respectively.

3.2. System Measurements

In this study, data were collected with a sampling time interval of about 2 s, and then recorded in a time series database as the average of the sampled values over a time interval of 5 min. In the rest of the manuscript, the following notation is adopted.

Let i be the integer index of the i-th time interval of day d in the monitored period, with $i = 1$ to k, while $t_{i,d}$ is the timestamp of the i-th time interval. Let $T_{i,d}$ be the duration of the i-th time interval of day d, where $T_{i,d} = t_{i,d} - t_{i-1,d}$. In this study, each i-th time interval has a constant time duration of 5 min (i.e., $T_{i,d} = T = 5$ min, $\forall\, i = 1$ to k, and $\forall\, d = 1$ to n), thus leading to a constant number of k intervals per day, with $k = 288$.

Let $P_{i,d}^{\mathrm{U}}$ be the average of the active power measured by the PCC power meter during the i-th time interval of day d. The sign convention for loads is applied to $P_{i,d}^{\mathrm{U}}$ measurements, i.e., with positive values representing the power absorbed from the grid and negative values representing the power fed into the grid.

Let $P_{i,d}^{\mathrm{PV}}$ be the average of the active power measured by the PV power meter during the i-th time interval of day d. The sign convention for generators is applied to $P_{i,d}^{\mathrm{PV}}$ measurements, which means that the power generated by the PV system is always positive.

Finally, let $P_{i,d}^{\mathrm{BESS}}$ be the average of the active power measured by the BESS PCS during the i-th time interval of day d. The sign convention for loads is applied to $P_{i,d}^{\mathrm{BESS}}$ measurements, i.e., with positive values representing the BESS charging power and negative values representing the BESS discharging power.

Based on the recorded measurements, the power demand of loads during the i-th time interval of day d, $P_{i,d}^{\mathrm{L}}$, considered by assuming the sign convention for loads, is computed by applying the power balance of the system, as defined by Equation (1).

$$P_{i,d}^{\mathrm{L}} = P_{i,d}^{\mathrm{PV}} + P_{i,d}^{\mathrm{U}} - P_{i,d}^{\mathrm{BESS}}, \tag{1}$$

4. Definition of the Metrics

In the following, the definition of the metrics is described in detail by separately presenting the metrics adopted to analyze the load profiles, PV generation profiles, and net power flow profiles. For the sake of comparison, the metrics for the evaluation of the energy balance of the prosumer's system are also presented.

4.1. Load Power Profile Metrics

Let $\overline{P}_i^{\mathrm{L}}$ be the average of the active power demand of loads during the i-th time interval, computed over all of the n days of the monitored period:

$$\overline{P}_i^{\mathrm{L}} = \sum_{d=1}^{n} \frac{P_{i,d}^{\mathrm{L}}}{n}, \tag{2}$$

Let $\sigma_{P_i^{\mathrm{L}}}$ be the standard deviation of the active power demand of loads during the i-th time interval, computed over all of the n days of the monitored period:

$$\sigma_{P_i^{\mathrm{L}}} = \sqrt{\frac{\sum_{d=1}^{n}\left(P_{i,d}^{\mathrm{L}} - \overline{P}_i^{\mathrm{L}}\right)^2}{n}}, \tag{3}$$

Let P_d^L be the daily average of the active power demand of loads of day d, computed over all of the k time intervals of the day:

$$P_d^L = \sum_{i=1}^{k} \frac{P_{i,d}^L}{k},$$ (4)

Let $\overline{P}_d^L$ be the average value of the daily average of the active power demand of loads, computed over all of the n days of the monitored period:

$$\overline{P}_d^L = \sum_{d=1}^{n} \frac{P_d^L}{n},$$ (5)

Let $\sigma_{P_d^L}$ be the standard deviation of the daily average active power demand of loads, computed over all of the n days of the monitored period:

$$\sigma_{P_d^L} = \sqrt{\frac{\sum_{d=1}^{n} \left(P_d^L - \overline{P}_d^L\right)^2}{n}},$$ (6)

Let $P_d^{L,max}$ be the daily peak of the active power demand of loads during day d, computed over all of the k time intervals:

$$P_d^{L,max} = max_i\left(P_{i,d}^L\right),$$ (7)

Let $\overline{P}_d^{L,max}$ be the average value of the daily peaks of the active power demand of loads, computed over all of the n days of the monitored period:

$$\overline{P}_d^{L,max} = \sum_{d=1}^{n} \frac{P_d^{L,max}}{n},$$ (8)

Let $\sigma_{P_d^{L,max}}$ be the standard deviation of the daily peak of the active power demand of loads, computed over all of the n days of the monitored period:

$$\sigma_{P_d^{L,max}} = \sqrt{\frac{\sum_{d=1}^{n} \left(P_d^{L,max} - \overline{P}_d^{L,max}\right)^2}{n}},$$ (9)

Let $P^{L,max}$ be the maximum value of the daily peak of the active power demand of loads, computed over all of the n days of the monitored period:

$$P^{L,max} = max_d\left(P_d^{L,max}\right),$$ (10)

Let $PR_{i,d}^L$ be the average of the absolute active power ramp of loads during the i-th time interval of day d:

$$PR_{i,d}^L = \frac{\left|P_{i,d}^L - P_{i-1,d}^L\right|}{T}, \ i = 2 \dots k,$$ (11)

Let $PR_d^{L,max}$ be the daily peak of the absolute power ramp of loads during day d:

$$PR_d^{L,max} = max_i\left(PR_{i,d}^L\right), \ i = 2 \dots k,$$ (12)

Let $\overline{PR_d^{L,max}}$ be the average of the daily peak of the absolute active power ramp of loads, computed over all of the n days of the monitored period:

$$\overline{PR_d^{L,max}} = \sum_{d=1}^{n} \frac{PR_d^{L,max}}{n}, \tag{13}$$

Let $\sigma_{PR_d^{L,max}}$ be the standard deviation of the daily peak of the absolute active power ramp of loads, computed over all of the n days of the monitored period:

$$\sigma_{PR_d^{L,max}} = \sqrt{\frac{\sum_{d=1}^{n}\left(PR_d^{L,max} - \overline{PR_d^{L,max}}\right)^2}{n}}, \tag{14}$$

Finally, let $PR^{L,max}$ be the maximum value of the daily peak of the absolute active power ramp of loads, computed over all of the n days of the monitored period:

$$PR^{L,max} = max_d\left(PR_d^{L,max}\right), \tag{15}$$

In Table 1, the summary of the metrics and related equations adopted to analyze the load profiles is briefly reported.

Table 1. Summary of the metrics and reference to the related equations adopted to analyze the load profiles. μ: average value, σ: standard deviation, max: maximum value.

Metric	μ (eq.)	σ (eq.)	max (eq.)
Active power demand of loads during the i-th time interval	$\overline{P_i^L}$ (2)	$\sigma_{P_i^L}$ (3)	−
Daily average of the active power demand of loads	$\overline{P_d^L}$ (5)	$\sigma_{P_d^L}$ (6)	$P_d^{L,max}$ (7)
Daily peak of the active power demand of loads	$\overline{P_d^{L,max}}$ (8)	$\sigma_{P_d^{L,max}}$ (9)	$P^{L,max}$ (10)
Daily peak of the absolute active power ramp of loads	$\overline{PR_d^{L,max}}$ (13)	$\sigma_{PR_d^{L,max}}$ (14)	$PR^{L,max}$ (15)

4.2. PV Power Profile Metrics

Let $\overline{P_i^{PV}}$ be the average of the PV active power generation during the i-th time interval, computed over all of the n days of the monitored period:

$$\overline{P_i^{PV}} = \sum_{d=1}^{n} \frac{P_{i,d}^{PV}}{n}, \tag{16}$$

Let $\sigma_{P_i^{PV}}$ be the standard deviation of the PV active power generation during the i-th time interval, computed over all of the n days of the monitored period:

$$\sigma_{P_i^{PV}} = \sqrt{\frac{\sum_{d=1}^{n}\left(P_{i,d}^{PV} - \overline{P_i^{PV}}\right)^2}{n}}, \tag{17}$$

Let P_d^{PV} be the daily average of the PV active power generation of day d, computed over all of the k time intervals of the day:

$$P_d^{PV} = \sum_{i=1}^{k} \frac{P_{i,d}^{PV}}{k}, \tag{18}$$

Let $\overline{P}_d^{\mathrm{PV}}$ be the average value of the daily average of the PV active power generation, computed over all of the n days of the monitored period:

$$\overline{P}_d^{\mathrm{PV}} = \sum_{d=1}^{n} \frac{P_d^{\mathrm{PV}}}{n}, \tag{19}$$

Let $\sigma_{P_d^{\mathrm{PV}}}$ be the standard deviation of the daily average PV active power generation, computed over all of the n days of the monitored period:

$$\sigma_{P_d^{\mathrm{PV}}} = \sqrt{\frac{\sum_{d=1}^{n} \left(P_d^{\mathrm{PV}} - \overline{P}_d^{\mathrm{PV}} \right)^2}{n}}, \tag{20}$$

Let $P_d^{\mathrm{PV},max}$ be the daily peak of the PV active power generation during day d, computed over all of the k time intervals:

$$P_d^{\mathrm{PV},max} = max_i \left(P_{i,d}^{\mathrm{PV}} \right), \tag{21}$$

Let $\overline{P}_d^{\mathrm{PV},max}$ be the average value of the daily peaks of the PV active power generation, computed over all of the n days of the monitored period:

$$\overline{P}_d^{\mathrm{PV},max} = \sum_{d=1}^{n} \frac{P_d^{\mathrm{PV},max}}{n}, \tag{22}$$

Let $\sigma_{P_d^{\mathrm{PV},max}}$ be the standard deviation of the daily peak of the PV active power generation, computed over all of the n days of the monitored period:

$$\sigma_{P_d^{\mathrm{PV},max}} = \sqrt{\frac{\sum_{d=1}^{n} \left(P_d^{\mathrm{PV},max} - \overline{P}_d^{\mathrm{PV},max} \right)^2}{n}}, \tag{23}$$

Let $P^{\mathrm{PV},max}$ be the maximum value of the daily peak of the PV active power generation, computed over all of the n days of the monitored period:

$$P^{\mathrm{PV},max} = max_d \left(P_d^{\mathrm{PV},max} \right), \tag{24}$$

Let $PR_{i,d}^{\mathrm{PV}}$ be the average of the absolute PV active power ramp during the i-th time interval of day d:

$$PR_{i,d}^{\mathrm{PV}} = \frac{\left| P_{i,d}^{\mathrm{PV}} - P_{i-1,d}^{\mathrm{PV}} \right|}{T}, \ i = 2 \dots k, \tag{25}$$

Let $PR_d^{\mathrm{PV},max}$ be the daily peak of the absolute PV active power ramp during day d:

$$PR_d^{\mathrm{PV},max} = max_i \left(PR_{i,d}^{\mathrm{PV}} \right), \ i = 2 \dots k, \tag{26}$$

Let $\overline{PR}_d^{\mathrm{PV},max}$ be the average of the daily peak of the absolute PV active power ramp, computed over all of the n days of the monitored period:

$$\overline{PR}_d^{\mathrm{PV},max} = \sum_{d=1}^{n} \frac{PR_d^{\mathrm{PV},max}}{n}, \tag{27}$$

Let $\sigma_{PR_d^{\mathrm{PV},max}}$ be the standard deviation of the daily peak of the absolute PV active power ramp, computed over all of the n days of the monitored period:

$$\sigma_{PR_d^{\mathrm{PV},max}} = \sqrt{\frac{\sum_{d=1}^{n}\left(PR_d^{\mathrm{PV},max} - \overline{PR}_d^{\mathrm{PV},max}\right)^2}{n}}, \tag{28}$$

Finally, let $PR^{\mathrm{PV},max}$ be the maximum value of the daily peak of the absolute PV active power ramp, computed over all of the n days of the monitored period:

$$PR^{\mathrm{PV},max} = max_d\left(PR_d^{\mathrm{PV},max}\right), \tag{29}$$

In Table 2, the summary of the metrics and related equations adopted to analyze the PV profiles is briefly reported.

Table 2. Summary of the metrics and reference to the related equations adopted to analyze the PV profiles. μ: average value, σ: standard deviation, max: maximum value.

Metric	μ (eq.)	σ (eq.)	max (eq.)
PV active power generation during the i-th time interval	$\overline{P}_i^{\mathrm{PV}}$ (16)	$\sigma_{P_i^{\mathrm{PV}}}$ (17)	−
Daily average of the PV active power	$\overline{P}_d^{\mathrm{PV}}$ (19)	$\sigma_{P_d^{\mathrm{PV}}}$ (20)	$P_d^{\mathrm{PV},max}$ (21)
Daily peak of the PV active power	$\overline{P}_d^{\mathrm{PV},max}$ (22)	$\sigma_{P_d^{\mathrm{PV},max}}$ (23)	$P^{\mathrm{PV},max}$ (24)
Daily peak of the absolute PV active power ramp	$\overline{PR}_d^{\mathrm{PV},max}$ (27)	$\sigma_{PR_d^{\mathrm{PV},max}}$ (28)	$PR^{\mathrm{PV},max}$ (29)

4.3. PCC Power Profile Metrics

Let $P_{i,d}^{\mathrm{U}^*}$ be the average active power flow at the PCC with the utility during the i-th time interval of day d, assuming that the BESS is not operating. This value can be computed from measured data by applying Equation (30):

$$P_{i,d}^{\mathrm{U}^*} = P_{i,d}^{\mathrm{U}} - P_{i,d}^{\mathrm{BESS}}, \tag{30}$$

Let $\overline{P}_i^{\mathrm{U}}$ ($\overline{P}_i^{\mathrm{U}^*}$) be the average of the active net power flow at the PCC during the i-th time interval, with (and without) the BESS in operation, computed over all of the n days of the monitored period:

$$\overline{P}_i^{\mathrm{U}} = \sum_{d=1}^{n} \frac{P_{i,d}^{\mathrm{U}}}{n}, \tag{31}$$

$$\overline{P}_i^{\mathrm{U}^*} = \sum_{d=1}^{n} \frac{P_{i,d}^{\mathrm{U}^*}}{n}, \tag{32}$$

Let $\sigma_{P_i^{\mathrm{U}}}$ ($\sigma_{P_i^{\mathrm{U}^*}}$) be the standard deviation of the active net power flow at the PCC during the i-th time interval, with (and without) the BESS in operation, computed over all of the n days of the monitored period:

$$\sigma_{P_i^{\mathrm{U}}} = \sqrt{\frac{\sum_{d=1}^{n}\left(P_{i,d}^{\mathrm{U}} - \overline{P}_i^{\mathrm{U}}\right)^2}{n}}, \tag{33}$$

$$\sigma_{P_i^{\mathrm{U}^*}} = \sqrt{\frac{\sum_{d=1}^{n}\left(P_{i,d}^{\mathrm{U}^*} - \overline{P}_i^{\mathrm{U}^*}\right)^2}{n}}, \tag{34}$$

Let $P_{i,d}^{\mathrm{FU}}$ ($P_{i,d}^{\mathrm{FU}^*}$) be the grid active power demand during the i-th time interval of day d, with (and without) the BESS in operation:

$$P_{i,d}^{\mathrm{FU}} = \begin{cases} P_{i,d}^{\mathrm{U}}, P_{i,d}^{\mathrm{U}} \geq 0 \\ 0, P_{i,d}^{\mathrm{U}} < 0 \end{cases}, \tag{35}$$

$$P_{i,d}^{\mathrm{FU}^*} = \begin{cases} P_{i,d}^{\mathrm{U}^*}, P_{i,d}^{\mathrm{U}^*} \geq 0 \\ 0, P_{i,d}^{\mathrm{U}^*} < 0 \end{cases}, \tag{36}$$

Let $P_d^{\mathrm{FU},max}$ ($P_d^{\mathrm{FU}^*,max}$) be the daily peak of the grid active power demand during day d, with (and without) the BESS in operation, computed over all of the k time intervals:

$$P_d^{\mathrm{FU},max} = max_i\left(P_{i,d}^{\mathrm{FU}}\right), \tag{37}$$

$$P_d^{\mathrm{FU}^*,max} = max_i\left(P_{i,d}^{\mathrm{FU}^*}\right), \tag{38}$$

Let $\overline{P}_d^{\mathrm{FU},max}$ ($\overline{P}_d^{\mathrm{FU}^*,max}$) be the average value of the daily peaks of the grid active power demand, with (and without) the BESS in operation, computed over all of the n days of the monitored period:

$$\overline{P}_d^{\mathrm{FU},max} = \sum_{d=1}^{n} \frac{P_d^{\mathrm{FU},max}}{n}, \tag{39}$$

$$\overline{P}_d^{\mathrm{FU}^*,max} = \sum_{d=1}^{n} \frac{P_d^{\mathrm{FU}^*,max}}{n}, \tag{40}$$

Let $\sigma_{P_d^{\mathrm{FU},max}}$ ($\sigma_{P_d^{\mathrm{FU}^*,max}}$) be the standard deviation of the daily peak of the grid active power demand, with (and without) the BESS in operation, computed over all of the n days of the monitored period:

$$\sigma_{P_d^{\mathrm{FU},max}} = \sqrt{\frac{\sum_{d=1}^{n}\left(P_d^{\mathrm{FU},max} - \overline{P}_d^{\mathrm{FU},max}\right)^2}{n}}, \tag{41}$$

$$\sigma_{P_d^{\mathrm{FU}^*,max}} = \sqrt{\frac{\sum_{d=1}^{n}\left(P_d^{\mathrm{FU}^*,max} - \overline{P}_d^{\mathrm{FU}^*,max}\right)^2}{n}}, \tag{42}$$

Let $P^{\mathrm{FU},max}$ ($P^{\mathrm{FU}^*,max}$) be the maximum value of the daily peak of the grid active power demand, with (and without) the BESS in operation, computed over all of the n days of the monitored period:

$$P^{\mathrm{FU},max} = max_d\left(P_d^{\mathrm{FU},max}\right), \tag{43}$$

$$P^{\mathrm{FU}^*,max} = max_d\left(P_d^{\mathrm{FU}^*,max}\right), \tag{44}$$

Let $P_{i,d}^{\mathrm{TU}}$ ($P_{i,d}^{\mathrm{TU}^*}$) be the active power grid feed during the i-th time interval of day d, with (and without) the BESS in operation:

$$P_{i,d}^{\mathrm{TU}} = \begin{cases} -P_{i,d}^{\mathrm{U}}, P_{i,d}^{\mathrm{U}} < 0 \\ 0, P_{i,d}^{\mathrm{U}} \geq 0 \end{cases}, \tag{45}$$

$$P_{i,d}^{\mathrm{TU}^*} = \begin{cases} -P_{i,d}^{\mathrm{U}^*}, P_{i,d}^{\mathrm{U}^*} < 0 \\ 0, P_{i,d}^{\mathrm{U}^*} \geq 0 \end{cases}, \tag{46}$$

Let $P_d^{\text{TU},max}$ $(P_d^{\text{TU}^*,max})$ be the daily peak of the active power grid feed during day d, with (and without) the BESS in operation, computed over all of the k time intervals:

$$P_d^{\text{TU},max} = max_i\left(P_{i,d}^{\text{TU}}\right),\tag{47}$$

$$P_d^{\text{TU}^*,max} = max_i\left(P_{i,d}^{\text{TU}^*}\right),\tag{48}$$

Let $\overline{P}_d^{\text{TU},max}$ $(\overline{P}_d^{\text{TU}^*,max})$ be the average value of the daily peaks of the active power grid feed, with (and without) the BESS in operation, computed over all of the n days of the monitored period:

$$\overline{P}_d^{\text{TU},max} = \sum_{d=1}^{n}\frac{P_d^{\text{TU},max}}{n},\tag{49}$$

$$\overline{P}_d^{\text{TU}^*,max} = \sum_{d=1}^{n}\frac{P_d^{\text{TU}^*,max}}{n},\tag{50}$$

Let $\sigma_{P_d^{\text{TU},max}}$ $(\sigma_{P_d^{\text{TU}^*,max}})$ be the standard deviation of the daily peak of the active power grid feed, with (and without) the BESS in operation, computed over all of the n days of the monitored period:

$$\sigma_{P_d^{\text{TU},max}} = \sqrt{\frac{\sum_{d=1}^{n}\left(P_d^{\text{TU},max} - \overline{P}_d^{\text{TU},max}\right)^2}{n}},\tag{51}$$

$$\sigma_{P_d^{\text{TU}^*,max}} = \sqrt{\frac{\sum_{d=1}^{n}\left(P_d^{\text{TU}^*,max} - \overline{P}_d^{\text{TU}^*,max}\right)^2}{n}},\tag{52}$$

Let $P^{\text{TU},max}$ $(P^{\text{TU}^*,max})$ be the maximum value of the daily peak of the active power grid feed, with (and without) the BESS in operation, computed over all of the n days of the monitored period:

$$P^{\text{TU},max} = max_d\left(P_d^{\text{TU},max}\right),\tag{53}$$

$$P^{\text{TU}^*,max} = max_d\left(P_d^{\text{TU}^*,max}\right),\tag{54}$$

Let $PR_{i,d}^{\text{U}}$ $(PR_{i,d}^{\text{U}^*})$ be the average of the absolute ramp of the active net power flow at the PCC during the i-th time interval of day d, with (and without) the BESS in operation:

$$PR_{i,d}^{\text{U}} = \frac{\left|P_{i,d}^{\text{U}} - P_{i-1,d}^{\text{U}}\right|}{T},\ i = 2\ldots k,\tag{55}$$

$$PR_{i,d}^{\text{U}^*} = \frac{\left|P_{i,d}^{\text{U}^*} - P_{i-1,d}^{\text{U}^*}\right|}{T},\ i = 2\ldots k,\tag{56}$$

Let $PR_d^{\text{U},max}$ $(PR_d^{\text{U}^*,max})$ be the daily peak of the absolute ramp of the net active power flow at the PCC during day d, with (and without) the BESS in operation:

$$PR_d^{\text{U},max} = max_i\left(PR_{i,d}^{\text{U}}\right),\ i = 2\ldots k,\tag{57}$$

$$PR_d^{\text{U}^*,max} = max_i\left(PR_{i,d}^{\text{U}^*}\right),\ i = 2\ldots k,\tag{58}$$

Let $\overline{PR}_d^{\mathrm{U},max}$ ($\overline{PR}_d^{\mathrm{U}^*,max}$) be the average of the daily peak of the absolute ramp of the net active power flow at the PCC, with (and without) the BESS in operation, computed over all of the n days of the monitored period:

$$\overline{PR}_d^{\mathrm{U},max} = \sum_{d=1}^{n} \frac{PR_d^{\mathrm{U},max}}{n},$$

(59)

$$\overline{PR}_d^{\mathrm{U}^*,max} = \sum_{d=1}^{n} \frac{PR_d^{\mathrm{U}^*,max}}{n},$$

(60)

Let $\sigma_{PR_d^{\mathrm{U},max}}$ ($\sigma_{PR_d^{\mathrm{U}^*,max}}$) be the standard deviation of the daily peak of the absolute ramp of the net active power flow at the PCC, with (and without) the BESS in operation, computed over all of the n days of the monitored period:

$$\sigma_{PR_d^{\mathrm{U},max}} = \sqrt{\frac{\sum_{d=1}^{n}\left(PR_d^{\mathrm{U},max} - \overline{PR}_d^{\mathrm{U},max}\right)^2}{n}},$$

(61)

$$\sigma_{PR_d^{\mathrm{U}^*,max}} = \sqrt{\frac{\sum_{d=1}^{n}\left(PR_d^{\mathrm{U}^*,max} - \overline{PR}_d^{\mathrm{U}^*,max}\right)^2}{n}},$$

(62)

Finally, let $PR^{\mathrm{U},max}$ ($PR^{\mathrm{U}^*,max}$) be the maximum value of the daily peak of the absolute ramp of the net active power flow at the PCC, with (and without) the BESS in operation, computed over all of the n days of the monitored period:

$$PR^{\mathrm{U},max} = max_d\left(PR_d^{\mathrm{U},max}\right),$$

(63)

$$PR^{\mathrm{U}^*,max} = max_d\left(PR_d^{\mathrm{U}^*,max}\right),$$

(64)

In the following tables, the summary of the metrics and related equations adopted to analyze the PCC active power flow profiles is briefly reported for each considered scenario, namely: without PV and storage (Scenario A, summarized in Table 3), with PV and without storage (Scenario B, summarized in Table 4, and with PV and storage (Scenario C, summarized in Table 5).

Table 3. Summary of the metrics and reference to the related equations adopted to analyze the net power profiles at the PCC with the utility for Scenario A, i.e., without PV and storage. μ: average value, σ: standard deviation, max: maximum value.

Metric	μ (eq.)	σ (eq.)	max (eq.)
Active net power flow at the PCC during the *i*-th time interval	$\overline{P}_i^{\mathrm{L}}$ (2)	$\sigma_{P_i^{\mathrm{L}}}$ (3)	–
Daily peak of grid power demand	$\overline{P}_d^{\mathrm{L},max}$ (8)	$\sigma_{P_d^{\mathrm{L},max}}$ (9)	$P^{\mathrm{L},max}$ (10)
Daily peak of grid power feed	–	–	–
Daily peak of the absolute ramp of the active net power flow at the PCC	$\overline{PR}_d^{\mathrm{L},max}$ (13)	$\sigma_{PR_d^{\mathrm{L},max}}$ (14)	$PR^{\mathrm{L},max}$ (15)

Table 4. Summary of the metrics and reference to the related equations adopted to analyze the net power profiles at the PCC with the utility for Scenario B, i.e., with PV and without storage. μ: average value, σ: standard deviation, max: maximum value.

Metric	μ (eq.)	σ (eq.)	max (eq.)
Active net power flow at the PCC during the i-th time interval	$\overline{P}_i^{\text{U}^*}$ (32)	$\sigma_{P_i^{\text{U}^*}}$ (34)	–
Daily peak of grid power demand	$\overline{P}_d^{\text{FU}^*,max}$ (40)	$\sigma_{P_d^{\text{FU}^*,max}}$ (42)	$P^{\text{FU}^*,max}$ (44)
Daily peak of grid power feed	$\overline{P}_d^{\text{TU}^*,max}$ (50)	$\sigma_{P_d^{\text{TU}^*,max}}$ (52)	$P^{\text{TU}^*,max}$ (54)
Daily peak of the absolute ramp of the active net power flow at the PCC	$\overline{PR}_d^{\text{U}^*,max}$ (60)	$\sigma_{PR_d^{\text{U}^*,max}}$ (62)	$PR^{\text{U}^*,max}$ (64)

Table 5. Summary of the metrics and reference to the related equations adopted to analyze the net power profiles at the PCC with the utility for Scenario C, i.e., with PV and storage. μ: average value, σ: standard deviation, max: maximum value.

Metric	μ (eq.)	σ (eq.)	max (eq.)
Active net power flow at the PCC during the i-th time interval	$\overline{P}_i^{\text{U}}$ (31)	$\sigma_{P_i^{\text{U}}}$ (33)	–
Daily peak of grid power demand	$\overline{P}_d^{\text{FU},max}$ (39)	$\sigma_{P_d^{\text{FU},max}}$ (41)	$P^{\text{FU},max}$ (43)
Daily peak of grid power feed	$\overline{P}_d^{\text{TU},max}$ (49)	$\sigma_{P_d^{\text{TU},max}}$ (51)	$P^{\text{TU},max}$ (53)
Daily peak of the absolute ramp of the active net power flow at the PCC	$\overline{PR}_d^{\text{U},max}$ (59)	$\sigma_{PR_d^{\text{U},max}}$ (61)	$PR^{\text{U},max}$ (63)

4.4. Prosumer's Energy Balance Metrics

Let SCR (SCR^*) be the self-consumption rate of the system, with (and without) the BESS in operation, computed over all of the n days of the monitored period. The SCR represents the rate of the energy produced by the PV system, which is directly consumed by the loads. The SCR and SCR^* are defined as follows:

$$SCR = \frac{\sum_{d=1}^n \sum_{i=1}^k min\left\{P_{i,d}^{\text{PV}} - P_{i,d}^{\text{BESS}}, P_{i,d}^{\text{L}}\right\} T_{i,d}}{\sum_{d=1}^n \sum_{i=1}^k P_{i,d}^{\text{PV}} T_{i,d}}, \tag{65}$$

$$SCR^* = \frac{min\left\{P_{i,d}^{\text{PV}}, P_{i,d}^{\text{L}}\right\} T_{i,d}}{\sum_{d=1}^n \sum_{i=1}^k P_{i,d}^{\text{PV}} T_{i,d}}, \tag{66}$$

Let SSR (SSR^*) be the self-sufficiency rate of the system, with (and without) the BESS in operation, computed over all of the n days of the monitored period. The SSR represents the rate of the energy consumed by the loads, which is directly provided by the PV system. The self-sufficiency rate estimates the independency of the prosumer from the power grid. The SSR and SSR^* are defined as follows:

$$SSR = \frac{\sum_{d=1}^n \sum_{i=1}^k min\left\{P_{i,d}^{\text{PV}} - P_{i,d}^{\text{BESS}}, P_{i,d}^{\text{L}}\right\} T_{i,d}}{\sum_{d=1}^n \sum_{i=1}^k P_{i,d}^{\text{L}} T_{i,d}}, \tag{67}$$

$$SCR^* = \frac{min\left\{P_{i,d}^{\text{PV}}, P_{i,d}^{\text{L}}\right\} T_{i,d}}{\sum_{d=1}^n \sum_{i=1}^k P_{i,d}^{\text{L}} T_{i,d}}, \tag{68}$$

5. Experimental Data

In this section, the data of the load active power demand and of the PV active power generation collected from 1 May 2020 to 31 May 2020 for the considered use case are reported and analyzed according to the metrics defined in Section 4.

5.1. Load Consumption Profile

In Figure 2 the active power demand profile of the loads is shown. Figure 2a shows the average power demand of loads for each *i*-th time interval (including the related standard deviation, shown by the red area) and peak power measurements. In Figure 2b, the standard deviation of the measurements for each *i*-th time interval is reported in detail.

(**a**) Average and maximum load demand   (**b**) Standard deviation of load demand
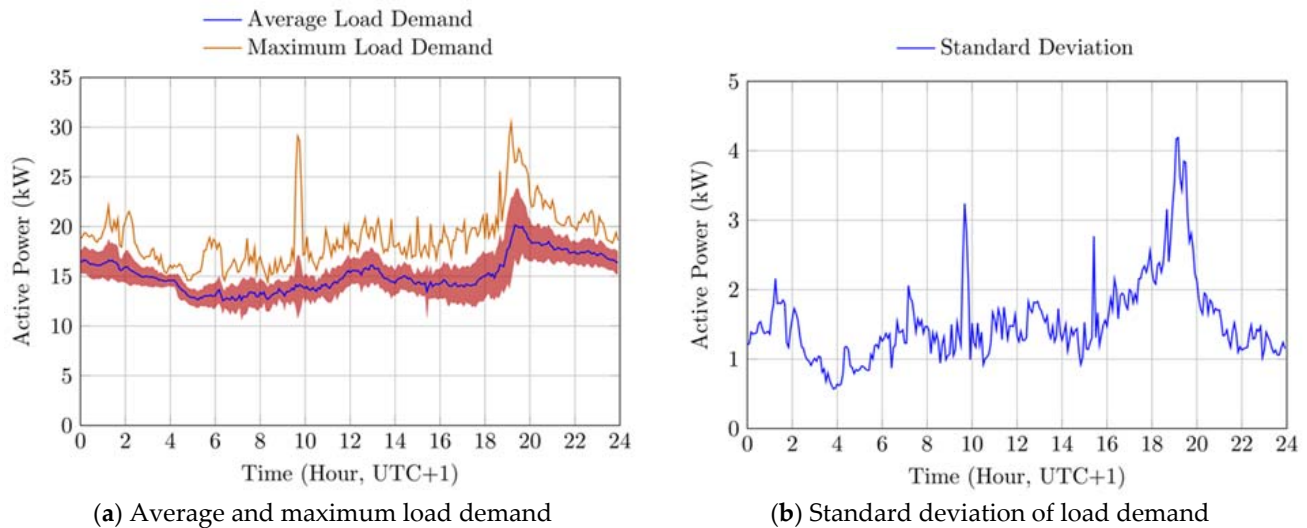
Figure 2. Active power demand profiles of loads during May 2020. In sub-figure (**a**), the red area represents the standard deviation of the measurements for each *i*-th time interval, which is reported in detail in sub-figure (**b**). UTC: universal time coordinated.

As can be noted from the charts of Figure 2, the active power demand of loads was almost constant during the day, with values close to 15 kW and a standard deviation between 1 and 2 kW. Only during the evening did the active power demand increase, reaching 20 kW. Two distinct peaks can be observed, both at 30 kW, at 10 AM and at 7 PM. The profile of the standard deviation of measurements for each *i*-th time interval exhibited a similar pattern by showing an increase during the evening (in correspondence to the increase of the average power demand) and two distinct peaks: one of about 3 kW at 10 AM and a larger peak of more than 4 kW at 7 PM.

In Table 6, the metrics for the synthetic evaluation of the active power demand of loads are reported in detail. As can be seen in the table, the daily average demand of loads was 15.2 kW, with a small standard deviation (only 0.7 kW, corresponding to about 5% of the average value) and a maximum value of 16.3 kW, corresponding to 107% of the average value.

Table 6. Metrics of the load demand profile during May 2020. μ: average value, σ: standard deviation, max: maximum value.

Metric	μ	σ	max
Daily average of the active power demand of loads (kW)	15.16	0.74	16.28
Daily peak of the active power demand of loads (kW)	23.16	2.8	30.42
Daily peak of the absolute active power ramp of loads (kW/min)	1.19	0.47	2.38

Concerning the daily peaks, it can be noted that the average value was 32.2 kW (i.e., 153% of the daily average demand), with a standard deviation of 2.8 kW, corresponding to about 12% of the average peak, and a maximum value of 30.4 kW, corresponding to 131% of the average peak. If compared to the average power consumption profiles, it can be noted that the daily profile of peaks exhibited a larger variability, particularly in terms of the recorded standard deviation of the peaks.

Finally, the analysis of the absolute active power ramp of loads showed that the average of the daily peaks was about 1.2 kW/min, with a standard deviation of 0.5 kW/min (corresponding to 39% of the average value), and with a maximum value of 2.4 kW/min, corresponding to 200% of the average value. It is worth noting that, even though the daily average of the absolute active power ramp of loads was relatively low if compared to the average consumption (i.e., less than 8%), its variability during the day was higher than the variability of the average power demand.

5.2. PV Production Profile

In Figure 3 the PV active power generation profile is shown. Figure 3a shows the average PV power generation for each *i*-th time interval (including the related standard deviation, shown by the red area) and peak power measurements. In Figure 3b, the standard deviation of the measurements for each *i*-th time interval is reported in detail.

(**a**) Average and maximum PV generation (**b**) Standard deviation of PV generation
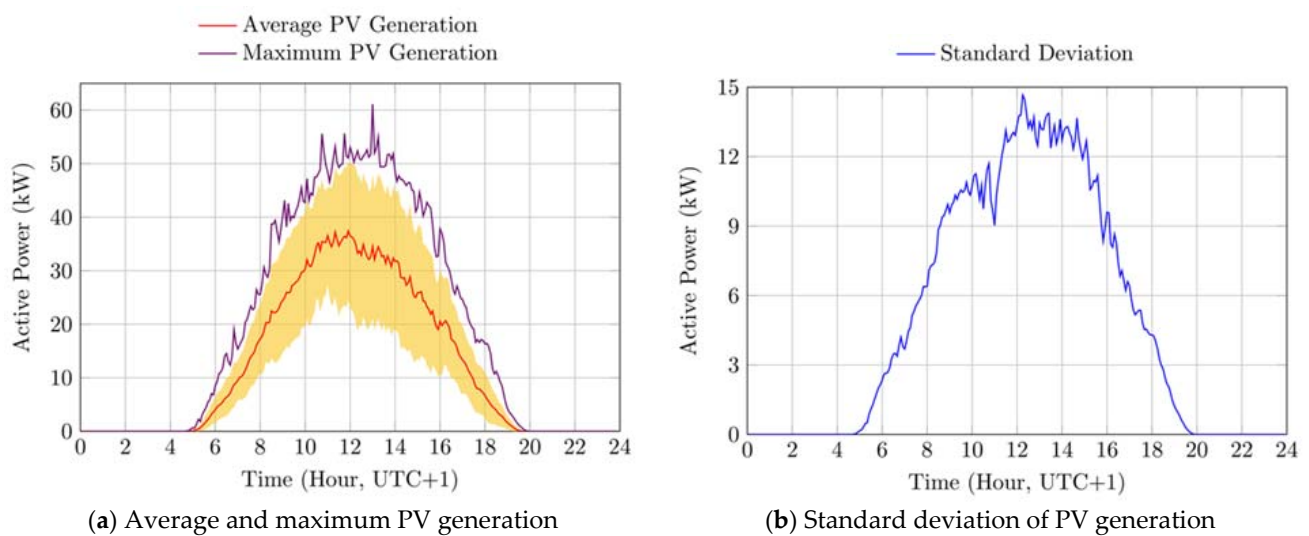
Figure 3. Active power generation profiles of the PV system during May 2020. In sub-figure (**a**), the red area represents the standard deviation of the measurements for each *i*-th time interval, which is reported in detail in sub-figure (**b**). UTC: universal time coordinated.

As is already known, the active power generation of the PV system varied largely during the day, following the typical sun path in the considered geographical location, with an average peak of production of about 47.2 kW and a maximum peak of 61.1 kW. It is worth noting that the standard deviation of the measurements for each *i*-th time interval almost exhibited the same pattern, with peaks close to 15 kW, corresponding to 31% of the average daily peak.

In Table 7 the metrics for the synthetic evaluation of the PV active power generation are reported in detail. As can be seen in the table, the daily average power generation of the PV system is 12 kW, with a standard deviation of 3.5 kW (corresponding to about 29% of the average value), and a maximum value of 16.4 kW, corresponding to 136% of the average value.

Table 7. Metrics of the PV generation profile during May 2020. μ: average value, σ: standard deviation, max: maximum value.

Metric	μ	σ	max
Daily average of the PV active power generation (kW).	12.03	3.46	16.41
Daily peak of the PV active power generation (kW)	47.25	6.54	61.12
Daily peak of the absolute PV active power ramp (kW/min)	4.31	1.75	7.3

Concerning the daily peaks, it can be noted that the average value was 47.2 kW (i.e., 393% of the daily average generation), with a standard deviation of 6.5 kW, corresponding to about 14% of the average peak, and a maximum value of 61.1 kW, corresponding to 129% of the average peak. The analysis of the absolute active power ramp of the PV power generation showed that the average of the daily peaks was about 4.3 kW/min, with a standard deviation of 1.7 kW/min (corresponding to 41% of the average value), and with a maximum value of 7.3 kW/min, corresponding to 169% of the average value. Finally, it can be noted that the ratio between the daily average of the absolute active power ramp of the PV system and the related average generation was equal to 36%, and that its variability was comparable to that of the average power generation.

5.3. Comparison of Load and PV Profiles

In Figure 4, the active power demand profile of loads and the active power generation profile of the PV system are compared.

(**a**) Average and maximum values   (**b**) Standard deviation
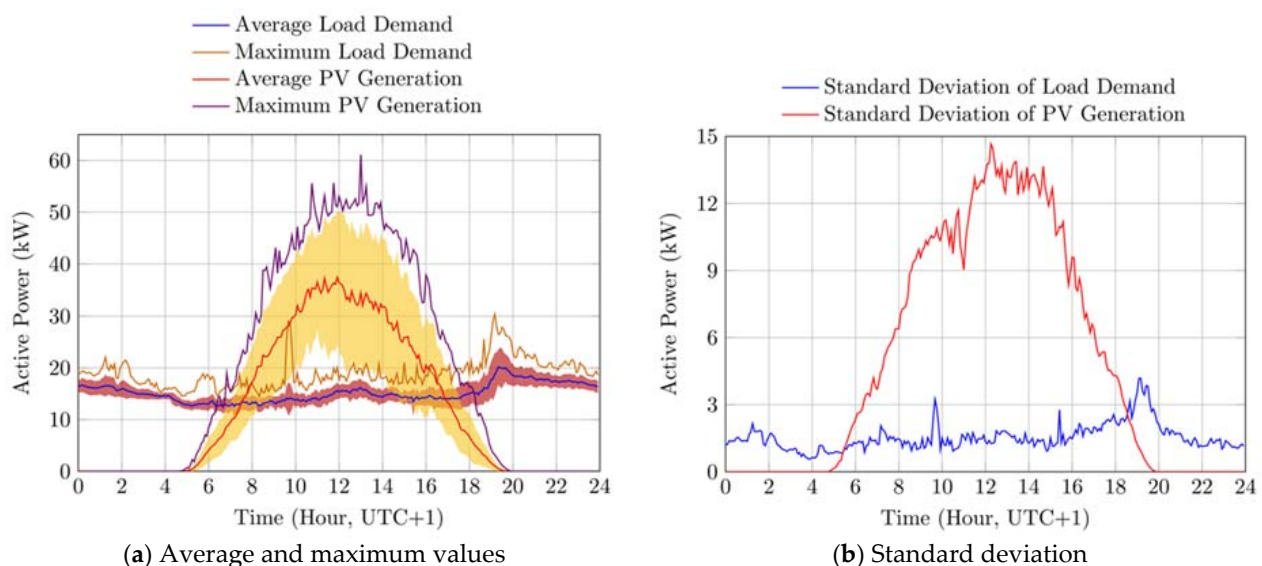
Figure 4. Active power demand profiles of loads and PV active power generation during May 2020. In sub-figure (**a**), the red and yellow areas represent the standard deviation of the measurements for each i-th time interval for the power demand of loads and the PV generation, respectively. The latter are reported in detail in sub-figure (**b**). UTC: universal time coordinated.

Figure 4a shows the average power demand of loads and the active power generation of the PV system, respectively, for each i-th time interval (including the related standard deviation, shown by the red and yellow areas, respectively) and peak power measurements. In Figure 4b, the standard deviation of the measurements for each i-th time interval are reported in detail for both of the loads and the PV system.

As can be noted from the charts of Figure 4, the pattern of the load demand profile and that of the PV generation profile showed (as expected) evidence of a large mismatch between power demand and generation, with the load profile showing an almost constant power demand during the day, and the PV profile showing the well-known bell shape. Besides that, of particular relevance is the difference between the variability of the two measured values, with the standard deviation of the PV active power generation being up to 20 times higher than the standard deviation of the average demand of loads, thus potentially leading to high increases in the variability of the net power flow at the PCC with the main grid, as shown in the following section.

6. Results and Discussion

This section presents the results of the analysis on the impact of the installation of the PV system and of the storage system on the prosumer's active net power profile. Three different scenarios are defined and then used to present the results of the analysis. Scenario A represents the case without PV and storage, and is used as the reference scenario in this analysis. Scenario B represents the introduction at the user's system of the PV power plant. Scenario B is analyzed in Section 6.1 to evaluate the impact of the PV installation on the active net power flows at the PCC, and will also serve as reference when analyzing the impact of the BESS. Scenario C, representing the introduction in combination with the PV system of the BESS operating with the rule-based control approach, is then analyzed in Section 6.2 to assess the effectiveness of the energy storage rule-based control in reducing the power flow uncertainties caused by the PV system. For the sake of comparison, the evaluation of the energy balance of the prosumer's system is finally provided in Section 6.3 by reporting the values of the SCR and SSR indicators for the considered use case with and without the operation of the BESS.

6.1. The Effect of PV on the End User's Power Profile

In Figure 5, the active net power flow at the PCC with the main grid for both Scenarios A and B is presented.

(**a**) Average active net power flow   (**b**) Standard deviation of active net power flow
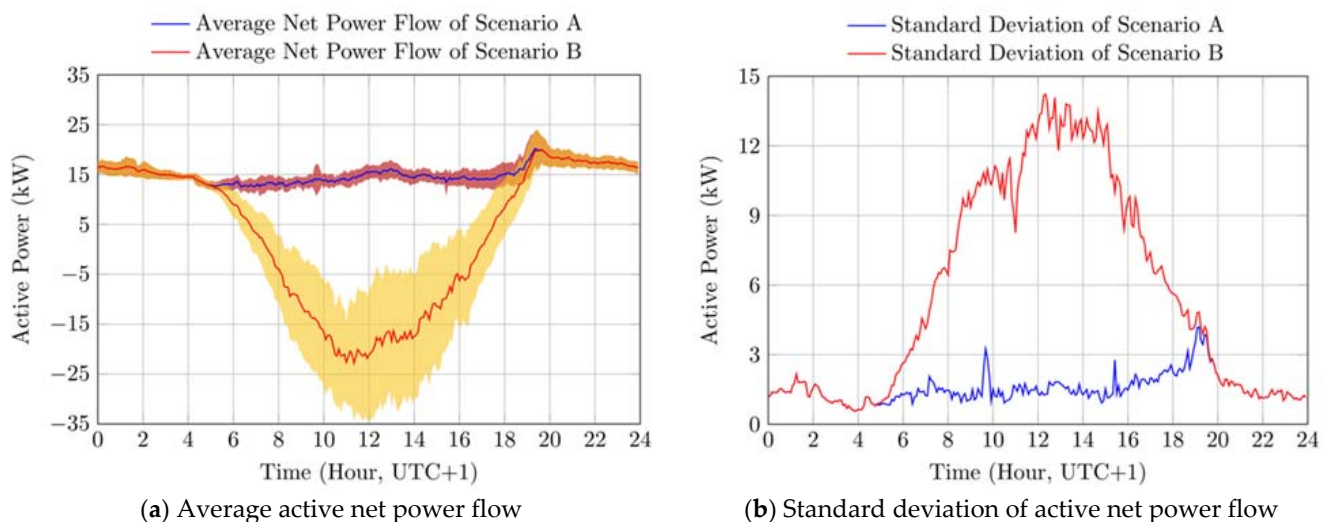
Figure 5. Active net power flow at the PCC with the main grid for Scenarios A and B during May 2020. In sub-figure (**a**), the red and yellow areas represent the standard deviation of the measurements for each *i*-th time interval for scenarios A and B, respectively. The latter are reported in detail in sub-figure (**b**). UTC: universal time coordinated.

Figure 5a shows the average active net power flow at the PCC for each *i*-th time interval (including the related standard deviation, shown by the red and yellow areas, for Scenario A and B, respectively), while Figure 5b depicts the standard deviation of the measurements for each *i*-th time interval.

As can be noted from the charts of Figure 5, the PV system had (as expected) a relevant impact on the shape and variability of the net active power flow at the PCC by introducing reverse power flows in the central part of the day, and by significantly increasing the uncertainty of the net active power values. This increase was evident during all of the hours of operation of the PV systems, and reached its maximum effect between 12 AM and 2 PM, where the recorded average standard deviation of the active net power flows reached the value of 13.14 kW for Scenario B, i.e., almost nine times higher than the value recorded for Scenario A, that is, 1.51 kW.

In Figure 6 the absolute power ramp of the active net power flow at the PCC with the main grid for both Scenarios A and B is presented. Figure 6a shows the average value

of the absolute power ramp and the related peak power measurements for each *i*-th time interval, while Figure 6b reports the standard deviation of the measurements.

(**a**) Average and maximum power ramps

(**b**) Standard deviation of power ramps
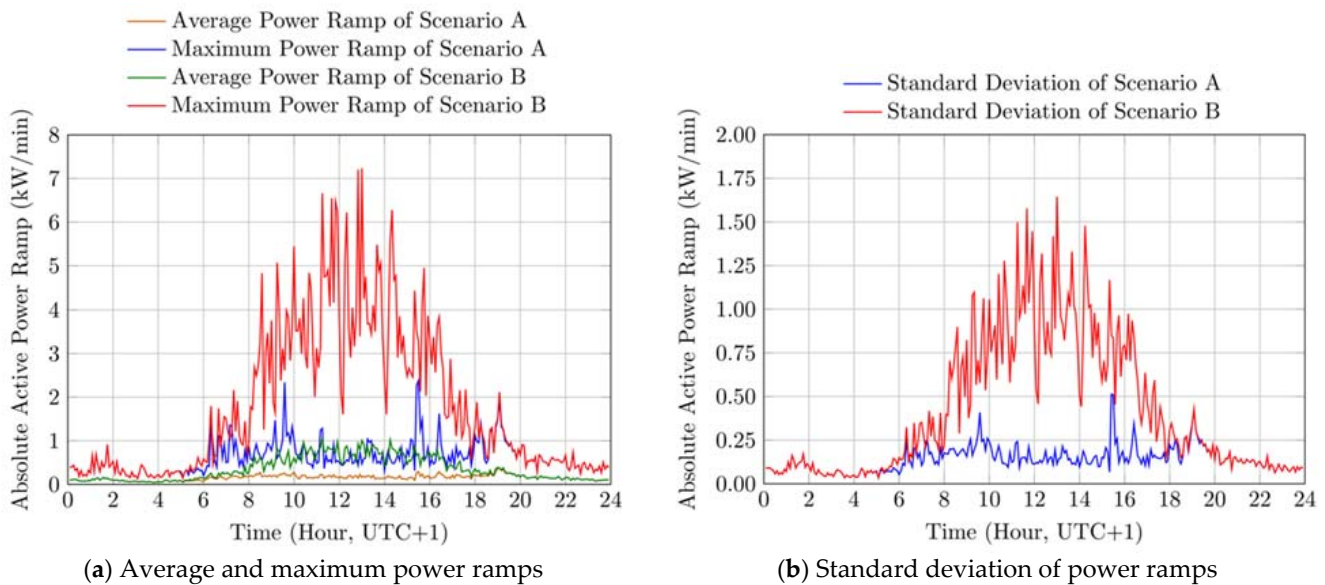
Figure 6. Absolute power ramp of the active net power flow at the PCC with the main grid for Scenarios A and B during May 2020. In sub-figure (**a**), the average and maximum values of the power ramp are shown, while sub-figure (**b**) reports the standard deviation of the measurements for each *i*-th time interval. UTC: universal time coordinated.

The charts depicted in Figure 6 show that, as noted for the active net power flow measurements, the operation of the PV system also had noticeable effects on the values of the absolute power ramps of the active net power flow at the PCC. If we consider the time interval between 12 AM and 2 PM, corresponding (statistically) to the period of maximum power generation of the PV system, the average power ramp during this time interval changed from 0.165 kW/min in Scenario A to 0.732 kW/min in Scenario B, i.e., more than four times higher, while the maximum power ramp recorded during the same time interval increased by almost seven times, from 1.038 kW/min in Scenario A to 7.232 kW/min in Scenario B. Similarly, the uncertainty of the power ramp also increased. In fact, the average standard deviation of the power ramp of Scenario A recorded during the time interval between 12 AM and 2 PM was 0.141 kW/min, while the value of Scenario B was 0.959 kW/min, i.e., almost seven times higher, and the maximum value was almost eight times higher, i.e., from 0.214 kW/min of Scenario A to 1.645 kW/min of Scenario B.

In Table 8 the metrics for the synthetic evaluation of the active net power flows at the PCC with the main grid for Scenario A and Scenario B are reported.

Table 8. Metrics of the active net power flow profile at the PCC with the main grid for Scenario A and B during May 2020. μ: average value, σ: standard deviation, max: maximum value.

Metric	Scenario A			Scenario B		
	μ	σ	max	μ	σ	max
Daily peak of the grid active power demand (kW)	23.16	2.8	30.42	22.85	2.66	30.16
Daily peak of the grid active power feed (kW)	0	0	0	32.63	6.14	46.26
Daily peak of the absolute ramp of the active net power flow at the PCC (kW/min)	1.19	0.47	2.38	4.27	1.69	7.23

To allow a direct evaluation of the effect of the PV system on the net active power flows, for each one of the three metrics reported in Table 8, the absolute and relative difference of the values of the metrics between Scenario B and Scenario A are reported in Tables 9–11, for the daily peak of the grid active power demand, the daily peak of the

grid active power feed, and the daily peak of the absolute ramp of the active net power flow, respectively.

Table 9. Variation of daily peak of the grid active power demand during May 2020 between Scenario B and Scenario A. μ: average value, σ: standard deviation, max: maximum value.

–	Absolute Difference (kW)	Relative Difference
μ	−0.31	−1.4%
σ	−0.13	−4.8%
max	−0.26	−0.9%

Table 10. Variation of daily peak of the grid active power feed during May 2020 between Scenario B and Scenario A. μ: average value, σ: standard deviation, max: maximum value.

–	Absolute Difference (kW)	Relative Difference
μ	32.63	–
σ	6.14	–
max	46.26	–

Table 11. Variation of daily peak of the absolute ramp of the active net power flow during May 2020 between Scenario B and Scenario A. μ: average value, σ: standard deviation, max: maximum value.

–	Absolute Difference (kW/min)	Relative Difference
μ	3.08	259.8%
σ	1.23	263.8%
max	4.85	204.1%

As can be noted by the results shown in the previous tables, the daily peak of the grid active power demand slightly decreased due to the contribution of the PV power generation, with a relative reduction on the order of a few % points. Conversely, the daily peak of the grid active power feed increased significantly, with an average value of about 32 kW, a standard deviation ±6.14 kW, and a maximum variation of 46.26 kW. Finally, particularly relevant was the impact on the daily peak of the absolute ramp of the active net power flow, which increased both in terms of the average value (that increased by almost 260%, with the maximum value by more than 200%) and the standard deviation of measurements, which increased by more than 260%.

6.2. The Effect of the PV-BESS Rule-Based Operation on the End User's Power Profile

In Figure 7 the active net power flow at the PCC with the main grid for all of the considered scenarios, namely Scenarios A, B, and C, is presented. Figure 7a shows the average active net power flow at the PCC for each *i*-th time interval, while Figure 7b reports the standard deviation of the measurements.

As can be noted by the charts of Figure 7, the storage system had controversial effects on the shape and variability of the net active power flow at the PCC.

The analysis of the variation of the average active net power flow in Figure 7a reveals that, from 6:30 AM to 8:30 AM, i.e., corresponding to the period of the day when, statistically, the BESS is in charge mode up to the moment it exceeds 90% of the SOC (i.e., approximately the limit of the constant current charge mode of Li-Ion batteries), the storage was able to avoid the occurrence of reverse power flow to the grid. Similarly, from 6 PM to 8 PM, i.e., corresponding to the period of the day when, statistically, the BESS is in discharge mode up to the moment it reaches the minimum allowed SOC value, the storage was able to reduce the power demand from the grid. Indeed, during the abovementioned time interval, the average power flow from the grid was reduced from 15.24 kW to 10.42 kW, that is, 68% of the original value.

(**a**) Average values

(**b**) Standard deviations
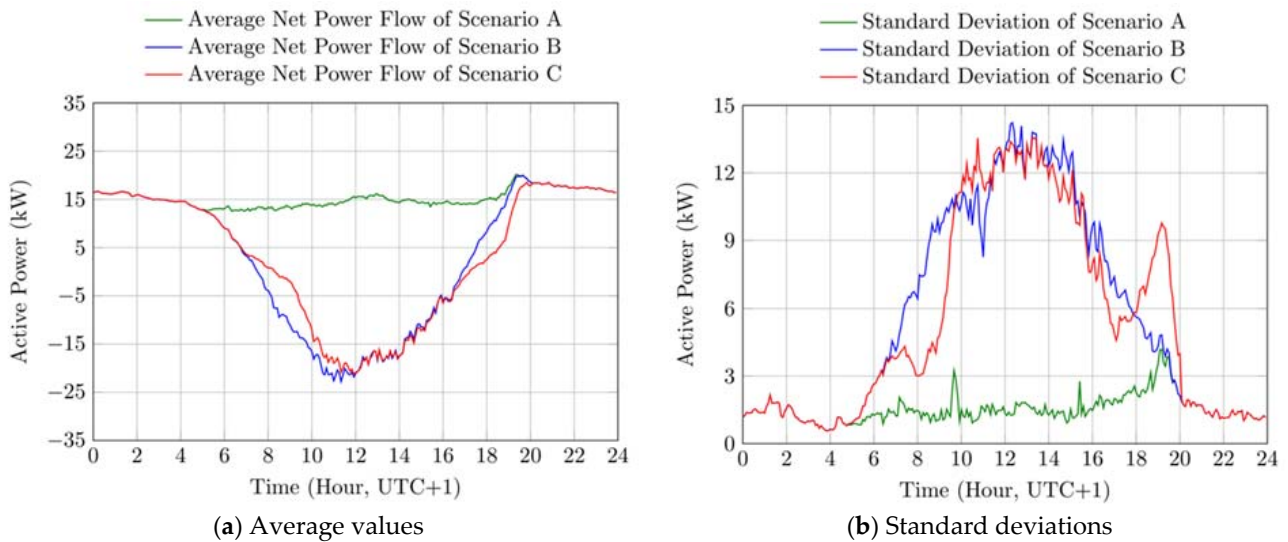
Figure 7. Active net power flow at the PCC with the main grid for Scenarios A, B, and C during May 2020. Sub-figure (**a**) shows the average value of the active net power flow, while sub-figure (**b**) reports the standard deviation of the measurements for each *i*-th time interval. UTC: universal time coordinated.

Looking at the curves depicted in Figure 7b, it can be noted that, from 6:30 AM to 8:30 AM, i.e., during the charge stage, the storage was able to reduce the uncertainty of the power flows, the average value of which changed from 5.88 kW of Scenario B to 3.66 kW of Scenario C, that is, 62% of the original value, while the maximum recorded value decreased from 8.77 kW to 4.32 kW, that is, 49% of the original value. Conversely, from 6 PM to 8 PM, i.e., during the discharge stage, the uncertainty of the power flows increased by showing a growth of the average value from 4.18 kW in Scenario B to 7.33 kW in Scenario C, that is, 175% of the original value, and, similarly, a rise of the maximum recorded value from 5.63 kW to 9.77 kW, corresponding to a relative growth of 173%.

In Figure 8 the absolute power ramp of the active net power flow at the PCC with the main grid for all of the considered scenarios, namely Scenarios A, B, and C, is presented. Figure 8a shows the average value of the absolute power ramp measurements for each *i*-th time interval, while in Figure 8b, the standard deviation of the measurements is reported.

(**a**) Average values

(**b**) Standard deviations
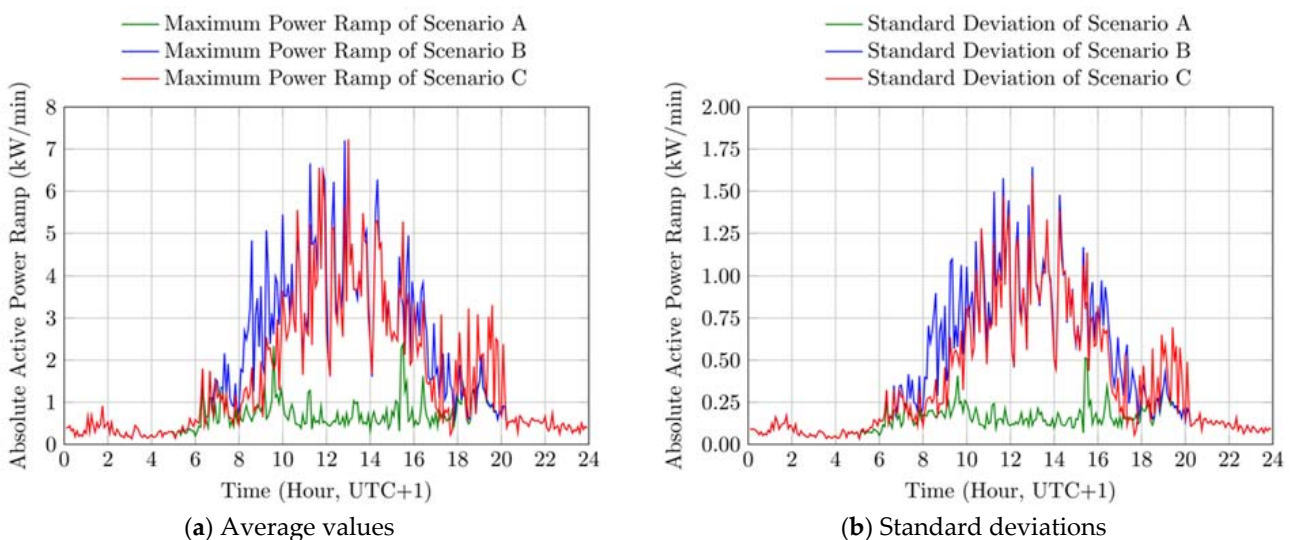
Figure 8. Absolute power ramp of the active net power flow at the PCC with the main grid for Scenarios A, B, and C during May 2020. In sub-figure (**a**), the average values of the power ramp are shown, while sub-figure (**b**) reports the standard deviation of the measurements for each *i*-th time interval. UTC: universal time coordinated.

Looking at the charts of Figure 8, it can be noted that the storage system had a positive impact on the shape and variability of the absolute power ramp of the net active power flow at the PCC, although showing controversial results during the discharge stage. Indeed, the operation of the storage system allowed the reduction of both the average and maximum values of the absolute power ramps during the charging stage, while relative increases in the variability of the power ramps was introduced during the discharge stage.

If we consider the time interval from 6:30 AM to 8:30 AM, the average value of the power ramp changed from 0.316 kW/min in Scenario B to 0.177 kW/min in Scenario C, that is, 56% of the original value, while the average of the recorded maximum values changed from 1.5 kW/min in Scenario B to 0.972 kW/min in Scenario C, that is, 65% of the original value, and the maximum recorded power ramp decreased from 3.23 kW to 1.744 kW, that is, 54% of the original value. Similarly, the average standard deviation of the power ramp during the charge stage decreased from 0.345 kW/min in Scenario B to 0.218 kW in Scenario C, that is, 63% of the original value, while the maximum deviation decreased from 0.778 kW/min to 0.327 kW/min, that is, 42% of the original value.

Controversial results, however, can be noted during the discharge stage. Indeed, if we consider the time interval from 6 PM to 8 PM, it can be noted that the average value of the power ramp decreased from 0.276 kW/min in Scenario B to 0.244 kW/min in Scenario C, that is, 88% of the original value, while the average of the recorded maximum values increased from 1.092 kW/min in Scenario B to 1.763 kW/min in Scenario C, that is, 161% of the original value, and the maximum recorded power ramp increased from 2.118 kW to 3.312 kW, that is, 161% of the original value. Similarly, the average standard deviation of the power ramp during the discharge stage increased from 0.248 kW/min in Scenario B to 0.375 kW in Scenario C, that is, 151% of the original value, while the maximum deviation increased from 0.429 kW/min to 0.695 kW/min, that is, 162% of the original value.

In Table 12 the metrics for the synthetic evaluation of the active net power flows at the PCC with the main grid for Scenario B and Scenario C are reported.

Table 12. Metrics of the active net power flow profile at the PCC with the main grid for Scenario B and C during May 2020. μ: average value, σ: standard deviation, max: maximum value.

	Scenario B			Scenario C		
Metric	μ	σ	**max**	μ	σ	**max**
Daily peak of the grid active power demand (kW)	22.85	2.66	30.16	22.41	2.64	30.18
Daily peak of the grid active power feed (kW)	32.63	6.14	46.26	30.87	8.48	46.23
Daily peak of the absolute ramp of the active net power flow at the PCC (kW/min)	4.27	1.69	7.23	3.86	1.4	7.23

To allow a direct evaluation of the effect of the storage system on the net active power flows, for each one of the three metrics reported in Table 12, the absolute and relative difference of the values of the metrics between Scenario C and Scenario B are reported in Tables 13–15, for the daily peak of the grid active power demand, the daily peak of the grid active power feed, and the daily peak of the absolute ramp of the active net power flow, respectively.

Table 13. Variation of the daily peak of the grid active power demand during May 2020 between Scenario C and Scenario B. μ: average value, σ: standard deviation, max: maximum value.

–	Absolute Difference (kW)	Relative Difference
μ	−0.44	−1.9%
σ	−0.03	−1%
max	0.02	0.1%

Table 14. Variation of the daily peak of the grid active power feed during May 2020 between Scenario C and Scenario B. μ: average value, σ: standard deviation, max: maximum value.

–	Absolute Difference (kW)	Relative Difference
μ	−1.76	−5.4%
σ	2.34	38.2%
max	−0.03	−0.1%

Table 15. Variation of daily peak of the absolute ramp of the active net power flow during May 2020 between Scenario C and Scenario B. μ: average value, σ: standard deviation, max: maximum value.

–	Absolute Difference (kW/min)	Relative Difference
μ	−0.41	−9.6%
σ	−0.3	−17.6%
max	0	0%

As can be noted by the results shown in the previous tables, the daily peak of the grid active power demand slightly decreased, with a relative reduction of almost 2%. Conversely, slightly better but also controversial results can be observed for the daily peak of the grid active power feed, the average value of which decreased by 5.4%, while its variability, i.e., its standard deviation, increased by almost 40%. Better results can be finally noted when evaluating the impact of the storage system on the daily peak of the absolute ramp of the active net power flow, the average value of which decreased by almost 10%, while its variability, i.e., its standard deviation, decreased by almost 18%.

6.3. The Effect of the PV-BESS Rule-Based Operation on the End User's Energy Balance

For the sake of comparison, the effect of the PV-BESS rule-based operation on the end user's energy balance is reported in Table 16 with and without the operation of the BESS, by referring to the self-consumption and self-sufficiency rates of the system (SCR and SSR, respectively). The results show that the BESS was able to increase both the SCR and the SSR by showing a relative increase of almost 11%, with the SCR increasing from 52.6% to 58.3%, and the SSR from 41.7% to 46.3%.

Table 16. Evaluation of the prosumer's energy balance during May 2020.

Metric	Without BESS	With BESS	Absolute Difference	Relative Difference
SCR	52.55%	58.27%	5.72%	10.89%
SSR	41.69%	46.34%	4.54%	10.89%

7. Conclusions

The results of the study showed that even though the BESS was able to increase the self-consumption and self-sufficiency of the system, with a relative increase of almost 11%, the impact of the SCR increase aimed, rule-based control approach had almost negligible effects on the uncertainty of the net power flows, while showing better results in terms of the reduction of the absolute power ramp.

Controversial effects have been observed in the variation of the uncertainty of the net power flows during the BESS charge and discharge stages. Indeed, during the charge stage, the average value of the standard deviation of the net active power flow at the PCC was reduced by a rate of 38%, while the same value increased by a rate of 75% during the discharge stage. Small but controversial effects were observed in terms of the variation of the peaks of the grid power demand and grid power feed and on the related variability. Globally, the effect of the BESS rule-based operation on the daily peaks of the grid power demand was very low, with a 2% decrease of the average demand peak and a 1% decrease of its standard deviation. Slightly better but also controversial results were observed for

the variation of the daily peaks of the grid power feed, the average value of which was reduced by 5.4%, while its standard deviation increased by almost 40%.

The most relevant positive impact was observed in the variation of the absolute power ramp of the active power flow at the PCC, the average value of which decreased by almost 10%, while its variability, i.e., its standard deviation, decreased by almost 18%. Particularly relevant was the effect during the BESS charge stages, where the average value of the absolute power ramp was reduced by 44%, with a 37% decrease of its average standard deviation (while the maximum recorded value decreased by a rate of 58%), and a 35% decrease of the average maximum value (while the maximum recorded value decreased by a rate of 46%). However, it must be also noted that even though the average value of the absolute power ramp during the discharge stage was reduced by 12%, its variability increased, with a relative rise of the average standard deviation of 51%, and a relative rise of the average of the maximum power ramps of 61%.

Finally, it must be noted that the small capacity of the BESS considered in this study, which is only 18% of the average excess of energy generation of the PV system, may have globally had an effect on the recorded results. However, the results observed for the BESS charging and discharging stages are not affected by this limitation, and represent an interesting point of discussion by suggesting that different storage control approaches should be investigated to reduce the uncertainty of net power flows in the presence of distributed PV systems.

Institutional Review Board Statement: Not applicable.

Informed Consent Statement: Not applicable.

Data Availability Statement: The data presented in this study are available on request from the corresponding author. The data are not publicly available due to privacy restrictions.

Conflicts of Interest: The author declares no conflict of interest.

References

1. Howell, S.; Rezgui, Y.; Hippolyte, J.L.; Jayan, B.; Li, H. Towards the next generation of smart grids: Semantic and holonic multi-agent management of distributed energy resources. *Renew. Sustain. Energy Rev.* **2017**, *77*, 193–214. [CrossRef]
2. Sharma, V.; Aziz, S.M.; Haque, M.H.; Kauschke, T. Effects of high solar photovoltaic penetration on distribution feeders and the economic impact. *Renew. Sustain. Energy Rev.* **2020**, *131*, 110021. [CrossRef]
3. Figgener, J.; Haberschusz, D.; Kaires, K.-P.; Wessels, O.; Zurmühlen, S.; Sauer, D.U. *Scientific Monitoring and Evaluation Program within the National Market Introduction Programm for PV-Home-Storage Systems. Wissenschaftliches Mess- und Evaluierungsprogramm Solarstromspeicher 2.0. Speichermonitoring BW-Jahresbericht 2019*; Aachen, Germany, 2019. Available online: https://www.researchgate.net/publication/335321329_Speichermonitoring_BW_-_Jahresbericht_2019 (accessed on 19 April 2021).
4. Namor, E.; Sossan, F.; Cherkaoui, R.; Paolone, M. Control of Battery Storage Systems for the Simultaneous Provision of Multiple Services. *IEEE Trans. Smart Grid* **2019**, *10*, 2799–2808. [CrossRef]
5. Xu, Y.; Wu, W.; Zhou, J. A Distributed Task Allocation Based on a Winner-Take-All Approach for Multiple Energy Storage Systems Coordination in a Microgrid. *IEEE Trans. Smart Grid* **2020**, *11*, 686–695. [CrossRef]
6. Taylor, Z.; Akhavan-Hejazi, H.; Cortez, E.; Alvarez, L.; Ula, S.; Barth, M.; Mohsenian-Rad, H. Customer-Side SCADA-Assisted Large Battery Operation Optimization for Distribution Feeder Peak Load Shaving. *IEEE Trans. Smart Grid* **2019**, *10*, 992–1004. [CrossRef]
7. Kucevic, D.; Tepe, B.; Englberger, S.; Parlikar, A.; Mühlbauer, M.; Bohlen, O.; Jossen, A.; Hesse, H. Standard battery energy storage system profiles: Analysis of various applications for stationary energy storage systems using a holistic simulation framework. *J. Energy Storage* **2020**, *28*, 101077. [CrossRef]
8. MacMackin, N.; Miller, L.; Carriveau, R. Investigating distribution systems impacts with clustered technology penetration and customer load patterns. *Int. J. Electr. Power Energy Syst.* **2021**, *128*, 106758. [CrossRef]
9. Al Essa, M.J.M. Power management of grid-integrated energy storage batteries with intermittent renewables. *J. Energy Storage* **2020**, *31*, 101762. [CrossRef]
10. Bartecka, M.; Barchi, G.; Paska, J. Time-series PV hosting capacity assessment with storage deployment. *Energies* **2020**, *13*, 2524. [CrossRef]

11. Marchi, B.; Zanoni, S.; Pasetti, M. A techno-economic analysis of Li-ion battery energy storage systems in support of PV distributed generation. In *21st Summer School F. Turco of Industrial Systems Engineering*; Italian Association of Industrial Operations Professors: Naples, Italy, 2016; pp. 145–149.

12. Marchi, B.; Pasetti, M.; Zanoni, S.; Zavanella, L.E. The Italian reform of electricity tariffs for non household customers: The impact on distributed generation and energy storage. In *22nd Summer School F. Turco of Industrial Systems Engineering*; Italian Association of Industrial Operations Professors: Palermo, Italy, 2017; pp. 103–109.

13. Sani Hassan, A.; Cipcigan, L.; Jenkins, N. Optimal battery storage operation for PV systems with tariff incentives. *Appl. Energy* **2017**, *203*, 422–441. [CrossRef]

14. Bendato, I.; Bonfiglio, A.; Brignone, M.; Delfino, F.; Pampararo, F.; Procopio, R.; Rossi, M. Design criteria for the optimal sizing of integrated photovoltaic-storage systems. *Energy* **2018**, *149*, 505–515. [CrossRef]

15. Liu, S.; Liu, P.X.; Wang, X.; Wang, Z.; Meng, W. Effects of correlated photovoltaic power and load uncertainties on grid-connected microgrid day-ahead scheduling. *IET Gener. Transm. Distrib.* **2017**, *11*, 3620–3627. [CrossRef]

16. Weitzel, T.; Glock, C.H. Energy management for stationary electric energy storage systems: A systematic literature review. *Eur. J. Oper. Res.* **2018**, *264*, 582–606. [CrossRef]

17. Baumann, M.; Weil, M.; Peters, J.F.; Chibeles-Martins, N.; Moniz, A.B. A review of multi-criteria decision making approaches for evaluating energy storage systems for grid applications. *Renew. Sustain. Energy Rev.* **2019**, *107*, 516–534. [CrossRef]

18. Sharma, R.; Karimi-Ghartemani, M. Addressing abrupt PV disturbances, and mitigating net load profile's ramp and peak demands, using distributed storage devices. *Energies* **2020**, *13*, 1024. [CrossRef]

19. Galván, L.; Navarro, J.M.; Galván, E.; Carrasco, J.M.; Alcántara, A. Optimal scheduling of energy storage using a new priority-based smart grid control method. *Energies* **2019**, *12*, 579. [CrossRef]

20. Ayodele, T.R.; Ogunjuyigbe, A.S.O.; Akpeji, K.O.; Akinola, O.O. Prioritized rule based load management technique for residential building powered by PV/battery system. *Eng. Sci. Technol. Int. J.* **2017**, *20*, 859–873. [CrossRef]

21. Jankowiak, C.; Zacharopoulos, A.; Brandoni, C.; Keatley, P.; MacArtain, P.; Hewitt, N. Assessing the benefits of decentralised residential batteries for load peak shaving. *J. Energy Storage* **2020**, *32*, 101779. [CrossRef]

22. Flammini, A.; Pasetti, M.; Rinaldi, S.; Bellagente, P.; Ciribini, A.L.C.; Tagliabue, L.C.; Zavanella, L.E.; Zanoni, S.; Oggioni, G.; Pedrazzi, G. A Living Lab and Testing Infrastructure for the Development of Innovative Smart Energy Solutions: The eLUX Laboratory of the University of Brescia. In Proceedings of the 110th AEIT International Conference (AEIT 2018), Bari, Italy, 3–5 October 2018.

23. Pasetti, M.; Rinaldi, S.; Flammini, A.; Longo, M.; Foiadelli, F. Assessment of Electric Vehicle Charging Costs in Presence of Distributed Photovoltaic Generation and Variable Electricity Tariffs. *Energies* **2019**, *12*, 499. [CrossRef]

24. Pasetti, M.; Rinaldi, S.; Manerba, D. A Virtual Power Plant Architecture for the Demand-Side Management of Smart Prosumers. *Appl. Sci.* **2018**, *8*, 432. [CrossRef]

25. Rinaldi, S.; Pasetti, M.; Flammini, A.; Ferrari, P.; Sisinni, E.; Simoncini, F. A Testing Framework for the Monitoring and Performance Analysis of Distributed Energy Systems. *IEEE Trans. Instrum. Meas.* **2019**, *68*, 1. [CrossRef]

26. Hesse, H.C.; Schimpe, M.; Kucevic, D.; Jossen, A. Lithium-Ion Battery Storage for the Grid—A Review of Stationary Battery Storage System Design Tailored for Applications in Modern Power Grids. *Energies* **2017**, *10*, 2107. [CrossRef]